

# Effects of solute-SIA binding energy on defect production behaviors in Fe-based alloys

Yaxuan Zhang <sup>a</sup>, Daniel Schwen <sup>b</sup>, Xian-Ming Bai <sup>a, b, \*</sup>

<sup>a</sup> Department of Materials Science and Engineering, Virginia Polytechnic Institute and State University, Blacksburg, VA, 24061, United States

<sup>b</sup> Fuel Modeling and Simulation Department, Idaho National Laboratory, Idaho Falls, ID, 83415, United States

## ARTICLE INFO

### Article history:

Received 20 March 2018

Received in revised form

25 May 2018

Accepted 18 June 2018

Available online 19 June 2018

### Keywords:

Primary damage

Solute-SIA binding energy

Solute interstitial fraction

Molecular dynamics

Fe-based alloys

## ABSTRACT

During primary damage, the fraction of produced solute interstitials in the total interstitials can be either higher or lower than the solute concentration in an alloy, depending on the solute type. To understand which alloy property governs the over- or under-production behaviors of solute interstitials, molecular dynamics simulations are conducted to simulate the cascade damage in a series of “artificial” Fe-Cr alloys with tunable binding energies between a substitutional solute (Cr) atom and a Fe self-interstitial atom (SIA). To achieve this, the Fe-Cr cross pair interaction in the interatomic potential is modified by multiplying a scaling factor so that the solute-SIA binding energy varies linearly from positive to negative values. It is found that the solute interstitial fraction has a strong correlation with the solute-SIA binding energy, and the correlation can be approximately described by a Fermi-Dirac-Distribution-like equation. The independent defect production results reported in literature are found to align well with this correlation. The correlation may be used to estimate the solute interstitial production behaviors in a wide range of Fe-based alloys simply based on the solute-SIA binding energy, without conducting laborious cascade simulations. It may also be used to improve the accuracy of predicting displacement per atom (dpa) of individual alloy constituents in the widely used SRIM software.

© 2018 Elsevier B.V. All rights reserved.

## 1. Introduction

Metallic alloys are important structural and cladding materials for both current and future reactors [1]. For example, iron-nickel-chromium (Fe-Ni-Cr) based austenitic steels are used as coolant pipe materials in light water reactors [2] and cladding materials in fast reactors [3]; Low-alloy Fe-based ferritic steels are used to manufacture reactor pressure vessels (RPV) in light water reactors [4]; Fe-Cr based ferritic/martensitic (F/M) steels, which have good thermal conductivities, coefficients of thermal expansion, and void swelling resistance, are proposed as cladding materials in next-generation fission reactors and first-wall materials and blankets in future fusion reactors [5,6]. Recently, high-entropy alloys and compositionally complex alloys have received significant interests for their potential applications in nuclear energy systems because

they exhibit good high-temperature mechanical strength, corrosion resistance, and radiation tolerance [7–10]. Under irradiation, the alloying (solute) elements in alloys can have both beneficial and detrimental effects on the materials performance. For instance, it has been shown that the void swelling in a Fe-12%Cr alloy is much smaller than that in a pure Fe under the same neutron irradiation conditions [11,12], indicating that the alloying element (i.e., Cr) in the Fe-Cr alloys can suppress the void growth. Similarly, the addition of different alloying elements in Ni-based alloys can dramatically reduce the void swelling and modify the spatial distribution of voids [9]. On the other hand, radiation can lead to segregation and precipitation of alloying elements [13]. In RPV steels, radiation can induce the precipitation of Cu-rich clusters and Mn-Ni-Si clusters [14–17], even though the concentrations of these alloying elements are very low. In Fe-Cr based F/M alloys, radiation can induce the precipitation of Cr-rich  $\alpha'$  phase [18,19]. Radiation can also cause the segregation of alloying elements to defect sinks such as grain boundaries [13,20]. These alloying-element-related microstructural evolution processes lead to radiation hardening and embrittlement in alloys [21]. Therefore, understanding how different alloying elements respond to radiation and their interactions with

\* Corresponding author. Department of Materials Science and Engineering, Virginia Polytechnic Institute and State University, Blacksburg, VA, 24061, United States.

E-mail address: [xmbai@vt.edu](mailto:xmbai@vt.edu) (X.-M. Bai).

point defects at the atomistic scale are critical for understanding the long-term microstructural evolution under irradiation.

Defect production by displacement cascades is the first step of radiation-induced microstructural evolution in materials. Molecular dynamics (MD) has been widely used to study cascade damage in various materials [22], including metallic alloys. For Fe-based alloys, the primary damage simulations were largely conducted in Fe-Cr binary alloys [23–29]. In these studies, researchers have used MD to investigate how the energy of the primary knock-on atom (PKA), solute (Cr) concentration, and temperature affect the defect production behaviors. Many studies [23,24,30] have shown that the number of total Frenkel pairs at the end of cascade recovery stage in Fe-based alloys is similar to that in a pure Fe, regardless of solute type or concentration (up to 15%). However, the ratio of solute interstitials (typically in the form of mixed dumbbells) in the total interstitials is not the same as the solute nominal concentration in the alloys. These results also show that the solute interstitial production efficiency, which is the normalized ratio of solute interstitials with respect to the solute nominal concentration in an alloy, is dramatically different from studies to studies, depending on the interatomic potentials used. Both over-production and under-production of solute interstitials have been reported. Some of the previous results are briefly summarized as follows. Terentyev et al. [25] and Malerba et al. [26] used an Embedded Atom Method (EAM) interatomic potential [31] to simulate the primary damage in a Fe-10%Cr alloy (in atomic percent) and found that the fraction of Fe-Cr mixed interstitial dumbbells is about 50–70% of the total interstitial dumbbells, or the Cr interstitial production efficiency is about 5–7. Svetukhin et al. [27] used the early version of the concentration-dependent EAM (CD-EAM) potential developed by Caro et al. [32] to simulate the primary damage in a Fe-9%Cr alloy and found that the Cr interstitial fraction is about 22%. Bjorkas et al. [28] used two different two-band embedded atomic model (2 BM) potentials and a one-band model (1 BM) potential to simulate the primary damage in a Fe-10%Cr alloy. The Cr interstitial fractions were found to be very close to the Cr concentration in the alloy (10%) using the 2 BM potentials, while only about 3% using the 1 BM potential. Later, Vortler et al. [23] used the same 2 BM potentials to study the primary damage in Fe-5%Cr, 10%Cr, and 15%Cr alloys and found that Cr interstitials are only over-produced in the Fe-5%Cr alloy. Shim et al. [29] used two different Finnis-Sinclair-type potentials to study the primary damage in a Fe-10%Cr alloy. The two potentials predict opposite signs of the binding energy between a Cr substitutional atom and a Fe self-interstitial atom (SIA). The results show that mixed Fe-Cr dumbbells (i.e., Cr interstitials) are over-produced when the Cr-SIA binding energy is positive and vice versa. In our recent work [24], we used the latter version of the CD-EAM potential developed by Stukowski et al. [33] to study the primary damage in Fe-5%Cr, Fe-10%Cr, and Fe-15%Cr alloys. Over-production of Cr interstitials was found in all of these alloys. The Cr interstitial production efficiency is about 3–6, and it decreases with the increasing Cr concentration. In contrast, in a Fe-5%Cu alloy, nearly no Cu interstitials were produced.

The previous explanations of the over-production of the solute (Cr) interstitials in Fe-Cr alloys were mainly based on the solute-trapping mechanism [25–27]. In this mechanism, if the solute-SIA binding energy is positive (attractive), fast-diffusing Fe SIAs can be trapped to form mixed interstitial dumbbells when they encounter solute atoms during the cascade recovery process. In our recent work [24], we differentiated two types of mixed dumbbells, namely, solute-interstitial-initiated and Fe-SIA-initiated ones, to elucidate the formation process of mixed dumbbells. In Fe-Cr alloys we found that the majority of the Fe-Cr mixed dumbbells are Cr interstitial-initiated ones, indicating that Cr interstitials form

directly and preferentially during the cascade recovery process. This is because a Cr interstitial has a lower formation energy in the Fe matrix than that of a Fe SIA. Therefore, their relative thermodynamic stability determines the over-production behavior of Cr interstitials. The solute-trapping mechanism, which results in Fe-SIA-initiated mixed dumbbells, still can contribute to the production of Fe-Cr mixed dumbbells. However, it does not play a major role. For Fe-Cu alloys, Cu interstitials are significantly under-produced because the formation energy of a Cu interstitial in the Fe matrix is much higher than that of a Fe SIA. In addition, we used an ideal/artificial potential to demonstrate that when the formation energies of a solute interstitial and a Fe SIA are the same, the solute interstitial fraction is very close to the solute nominal concentration in the alloy. It is worth noting that the difference in formation energy between a Fe SIA and a solute interstitial is actually the binding energy between a substitutional solute atom and a Fe SIA [24]. Therefore, regardless of the detailed formation mechanisms of mixed dumbbells discussed above, the solute-SIA binding energy is likely to be the main factor that governs the over- and under-production behaviors of solute interstitials. This hypothesis is supported by the aforementioned Shim et al.'s work [29]. It is also supported by our previous work [24] that distinct solute interstitial production behaviors were observed in Fe-Cr (positive binding energy between Cr-SIA) and Fe-Cu (negative binding energy between Cu-SIA) alloys.

Although the sign of the solute-SIA binding energy may be used as an indicator to qualitatively predict the over- or under-production behaviors of solute interstitials in Fe-based alloys, the quantitative correlation between them has not been established to date. Establishing such a correlation is beneficial because we may use it to quantitatively or semi-quantitatively predict the solute interstitial fraction simply based on the solute-SIA binding energy for a wide range of Fe-based alloys without performing the laborious cascade simulations. In this work, we use a tunable potential to study the solute interstitial production behaviors in Fe-based alloys, in which the Fe-solute (Cr) cross pair interaction is multiplied by a scaling factor. These modified potentials derived from the tunable potential can predict a wide range of solute-SIA binding energies but keep other interaction terms as same as in the original potential. This approach will minimize the factors that may influence the defect production behaviors and enable us to focus on the correlation between the solute interstitial fraction and the solute-SIA binding energy.

## 2. Simulation methods

In this work, the LAMMPS software [34] was used to conduct MD simulations of cascade-induced primary damage in both “real” and “artificial” Fe-Cr alloys. To model the “real” Fe-Cr system, the CD-EAM potential developed by Stukowski et al. [33] was used. This potential correctly predicts the change of sign in the heat of mixing curve [24], which agrees with the DFT calculations [35]. This potential also correctly predicts that a <110> SIA dumbbell is more stable than a <111> SIA dumbbell in a pure Fe. To model the “artificial” Fe-Cr alloys, the cross pair interaction between a Fe atom and a Cr atom in the CD-EAM potential was modified by multiplying a scaling factor (SF),  $\chi$ ,

$$\phi'_{\text{Fe-Cr}} = \phi_{\text{Fe-Cr}} \cdot \chi, \quad (1)$$

where  $\chi$  ranges from 0.7 to 1.3. All other interaction terms were the same as in the original potential. By adjusting the scaling factor  $\chi$  in Eq. (1), a series of interatomic potentials were created with tunable properties. As shown in the next Section, the binding energy between a Cr substitutional atom and a Fe SIA predicted by these

potentials decreases nearly linearly from positive to negative values with the increasing scaling factor. Note that the properties of the pure components (Fe and Cr) in these potentials are unaffected. Therefore, the use of these modified potentials can help us minimize the factors that may affect the defect production behaviors, and determine which factor governs these behaviors in alloys. In addition to the modified Fe–Cr potentials, an EAM potential for Fe–Cu–Ni systems [36] was used to study the defect production in a Fe–5%Cu and a Fe–5%Ni, aiming at validating whether the conclusions obtained from the artificial Fe–Cr alloys can be extended to other realistic Fe-based alloys. To describe the short-range repulsive interaction between atoms during cascade simulations, all the pair interaction terms in each potential were smoothly splined to the Ziegler–Biersack–Littmark (ZBL) potential [37] at the interatomic distance of 1.2 Å.

All cascade simulations were performed at 300 K and the simulation boxes had a cubic geometry. The PKA direction was set to the [135] direction in each simulation. For cubic crystals, this PKA direction is typically used to represent the average defect production behaviors of all crystallographic orientations [22]. The cascade simulation conditions such as PKA energy, number of atoms, simulation box size, number of simulations, Cr concentration, simulation time are summarized in Table 1. Here we mainly used random Fe–3%Cr, Fe–5%Cr, and Fe–10%Cr alloys. These alloy systems were created by substituting Fe atoms with Cr atoms randomly in a Fe matrix. Periodic boundary conditions were employed in all dimensions. In each cascade simulation, initially the simulation system was equilibrated at 300 K in a constant number of atom, constant volume, and constant temperature (NVT) ensemble for about 6 ps and the velocity rescaling method was used to control the temperature of the entire system. Then the velocity rescaling was only applied to the atoms within a thin layer of 2.9 Å from the simulation box boundaries for dissipating the cascade energy. The PKA was a Fe atom near the center of the simulation box in each simulation. The PKA energy ranges from 2 keV to 20 keV and the system size increases with the PKA energy, as shown in Table 1. After the recoil was initiated in each simulation, the system was allowed to evolve for another 47–57 ps, depending on the PKA energy (Table 1). The final damaged structure at the end of the simulation was used for defect analysis. Typically, 20–30 independent simulations were conducted for each simulation condition to get statistical meaningful results. To characterize defects (interstitials and vacancies), the reference lattice site method was used. The cutoff distance for defining a defect in this method was set to 0.9 Å. To obtain the net number of defects in a cluster, a cluster analysis method was used to cancel interstitial–vacancy pairs of the same species within a cluster. In this method if the distance between any two defects is less than 2.5 Å, they are assigned to the same cluster. For example, a split interstitial dumbbell consists of two interstitials centered with one vacancy. Using this cluster analysis method, the split interstitial dumbbell is counted as one interstitial and its type (Fe SIA or solute interstitial) depends on the central vacancy type. The details of the two methods can be found in Refs. [24,38,39].

### 3. Results

#### 3.1. Defect energetics in dilute alloys

In our previous work [24], we have demonstrated that the relative thermodynamic stability between a solute interstitial and a matrix SIA, which is the difference in their formation energies, is the most important factor for determining over- or under-production behavior of solute interstitials in alloys. If a solute interstitial has a lower formation energy in the Fe matrix than that of a SIA, solute interstitials form directly and preferentially during the cascade recovery stage. This mechanism is different from the commonly assumed solute trapping mechanism in which a SIA is trapped by a solute atom during its fast gliding [25–27]. Since the cross pair interaction between a Fe atom and a Cr atom (Eq. (1)) is modified in the tunable potential, the Cr interstitial formation energy also changes with the scaling factor of the Fe–Cr pair interaction. The formation energy of a Cr interstitial in a Fe matrix is defined as,

$$E_f = E_{\text{defect}} - E_{\text{perfect}} - \varepsilon_{\text{Fe}}, \quad (2)$$

where  $E_{\text{defect}}$  is the total energy of a Fe matrix containing a Cr interstitial,  $E_{\text{perfect}}$  is the total energy of a Fe matrix containing a substitutional Cr atom, and  $\varepsilon_{\text{Fe}}$  is the cohesive energy per atom of a pure Fe. The formation energy of a Cr interstitial as a function of the scaling factor is shown in Fig. 1, which increases almost linearly with the scaling factor from 2.69 eV to 3.85 eV. The Cr interstitial formation energy predicted by the original CD-EAM potential (at SF = 1.0) is 3.3 eV. The linear increase of the Cr interstitial formation energy indicates that formation of Cr interstitials becomes more and more difficult as the scaling factor increases.

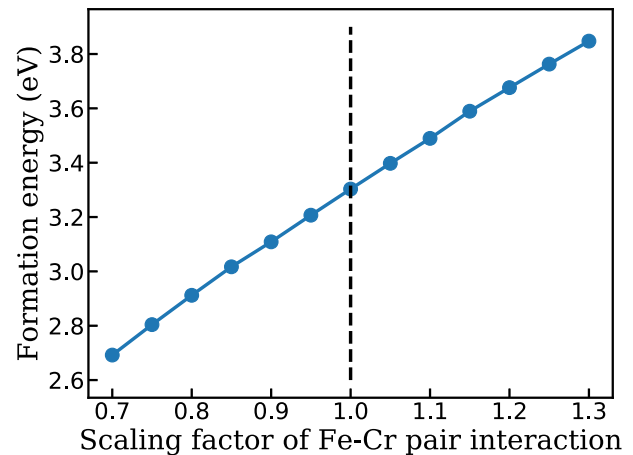
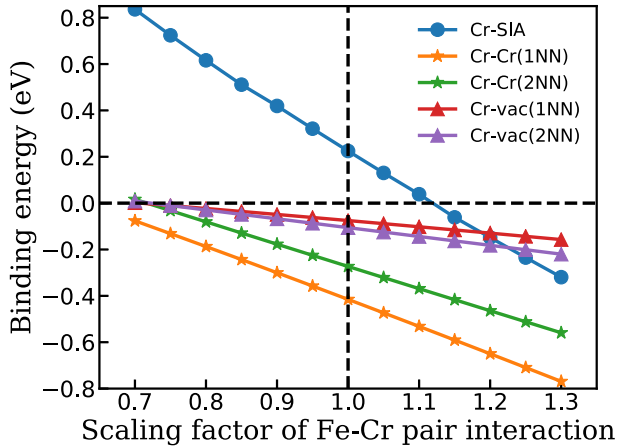


Fig. 1. Formation energy of a Cr interstitial in a Fe matrix as a function of the scaling factor of the Fe–Cr cross pair interaction in the tunable interatomic potential. The formation energy indicated by the dash line is the value predicted by the original CD-EAM potential.

**Table 1**  
System configurations and simulation conditions in cascade simulations. In all simulations the temperature was set to 300 K and the PKA direction was along the [135] direction. The lattice parameter  $a_0 = 2.86$  Å.

PKA energy (keV)	System size (atoms)	Side length of simulation box (in $a_0$ )	Number of simulations	Cr concentration	Total simulation time (ps)
2	54,000	30	30	3%,5%,10%	53
5	128,000	40	30	3%,5%,10%	53
10	432,000	60	20	3%,5%,10%	63
20	432,000	60	20	3%,5%,10%	63



**Fig. 2.** The Cr-defect and Cr-Cr binding energies in dilute Fe-Cr alloys as a function of the scaling factor of Fe-Cr cross pair interaction predicted by the tunable potential (Eq. (1)).

The binding energies of a solute (Cr) atom with point defects as well as with another solute atom are calculated in dilute Fe-Cr alloys, which are defined as

$$E_b = E_{\text{separate}} - E_{\text{complex}}, \quad (3)$$

where  $E_{\text{separate}}$  is the total energy of the system containing both a solute and a defect (or another solute) at a well-separated distance;  $E_{\text{complex}}$  is the total energy of the system containing a close solute-defect or a solute-solute pair. Here a positive binding energy means that a solute atom tends to bind with a defect or another solute atom, and vice versa. The calculated binding energies of different types of pairs as a function of the scaling factor are shown in Fig. 2. The vertical black dash line at SF = 1.0 indicates the binding energies predicted by the original CD-EAM potential for these pairs. For the binding energy between a substitutional Cr atom and a Fe SIA ( $E_b^{\text{Cr-SIA}}$ ), it decreases approximately linearly from a positive to a negative value as the SF increases. At about SF = 1.1,  $E_b^{\text{Cr-SIA}}$  has a nearly zero value. Therefore, the modified potentials (which are generated from the tunable potential) can predict positive, zero, and negative values in Cr-SIA binding energy, which can help elucidate the role of  $E_b^{\text{Cr-SIA}}$  on the over- or under-production behavior of Cr interstitials. We do notice that the binding energies of a Cr-Cr solute pair and a Cr-vacancy pair at both 1st and 2nd nearest neighbor distances also decrease with the increasing scaling factor, as shown in Fig. 2. These changes are a little counter-intuitive, because only the Fe-Cr pair interaction is modified in these potentials. The reason is that Cr atoms are dilute in the Fe matrix. Therefore, the binding energy of a Cr-Cr pair is affected not only by the unmodified Cr-Cr pair interaction, but also by the modified Fe-Cr pair interaction. Similar argument can also be applied to the binding energy of a Cr-vacancy pair. The changes of the Cr-Cr and Cr-vacancy binding energies may slightly influence the defect production behaviors. However, it is expected that these changes do not affect the production behaviors of solute (Cr) interstitials significantly because a Cr interstitial typically has a Fe-Cr mixed interstitial dumbbell structure. Therefore, the Cr-SIA binding energy should be more relevant to the solute interstitial production behaviors.

Since the only thing changed in these modified potentials is the Fe-Cr pair interaction, the formation energy of a Fe SIA remains unchanged, which is 3.53 eV. The Cr-SIA binding energy is simply the difference in the formation energy between a Cr interstitial and a Fe SIA,

$$E_b^{\text{Cr-SIA}} = E_f(\text{SIA}) - E_f(\text{Cr int}). \quad (4)$$

Therefore, the Cr interstitial formation energy shown in Fig. 1 can be correlated to the Cr-SIA binding energy shown in Fig. 2. A low formation energy corresponds to a high binding energy and vice versa.

### 3.2. Heat of mixing

It is expected that these modified potentials change the heat of mixing curve of the Fe-Cr alloy system. Assuming in a Fe-Cr alloy the atomic fraction of Cr is  $x_{\text{Cr}}$ , the heat of mixing can be calculated by,

$$\Delta H_{\text{mix}} = \epsilon_{\text{alloy}} - (1 - x_{\text{Cr}}) \times \epsilon_{\text{Fe}} - x_{\text{Cr}} \times \epsilon_{\text{Cr}}, \quad (5)$$

where  $\epsilon_{\text{alloy}}$  is the internal energy per atom in the Fe- $x_{\text{Cr}}$ -Cr alloy system with randomly distributed Cr solute atoms, and  $\epsilon_{\text{Fe}}$  and  $\epsilon_{\text{Cr}}$  are the internal energies per atom (cohesive energies) of pure Fe and pure Cr, respectively. Here the heat of mixing curves of Fe-Cr alloys predicted by the original (SF = 1.0) and three modified potentials (SF = 0.9, 1.1, and 1.2) are calculated, as shown in Fig. 3. For the original CD-EAM potential, the sign of the heat of mixing changes from negative to positive at about  $x_{\text{Cr}} = 0.1$ , which is consistent with DFT calculations [35]. For the modified potential with SF = 0.9, it predicts a positive heat of mixing curve in the complete composition range, which is similar to the Fe-Cu system [24]. At any given  $x_{\text{Cr}}$ , it predicts a larger heat of mixing than the original potential. For those potentials with SF < 0.9, they predict more positive heat of mixing than the potential with SF = 0.9 at every Cr concentration. For the potential with SF = 1.1, the predicted heat of mixing is negative at most Cr concentrations and slightly positive at  $x_{\text{Cr}} > 0.65$ . For the potential with SF = 1.2, the predicted heat of mixing remains negative at all compositions. Therefore, as the scaling factor increases, the heat of mixing becomes more negative. For the Fe-10%Cr alloy studied in this work, the heat of mixing has positive, nearly zero, and negative values as the SF increases. The different heats of mixing at the same alloy composition may help us investigate the effect of heat of mixing on the defect production behaviors.

### 3.3. Number of total Frenkel pairs

To investigate how these modified potentials affect the

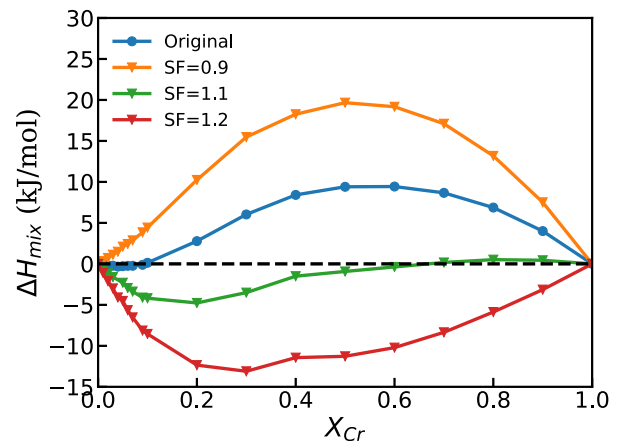


**Fig. 3.** Heat of mixing curves of a series of “Fe-Cr” systems predicted by the original CD-EAM potential (SF = 1.0) and three modified potentials (SF = 0.9, 1.1, 1.2).



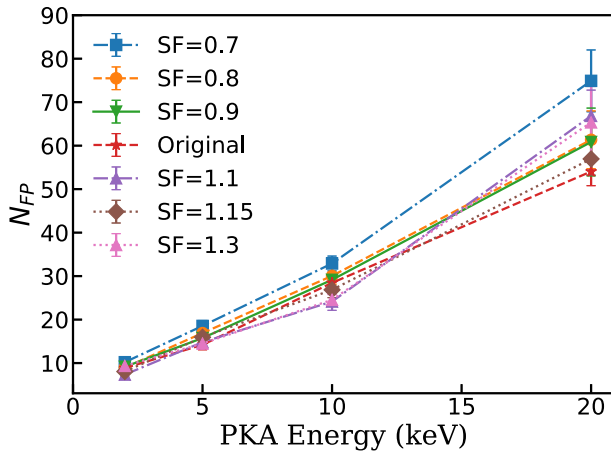


**Fig. 4.** The numbers of total surviving Frenkel pairs ( $N_{FP}$ ) at the end of cascade simulations in a Fe-10%Cr alloy as a function of PKA energy predicted by the modified potentials of different scaling factors. The error bars represent standard errors.

production behavior of Frenkel pairs, the numbers of total Frenkel pairs (interstitial-vacancy pairs) at the end of cascade simulations are obtained in a Fe-10%Cr alloy using the modified potentials of different scaling factors. The PKA energy ranges from 2 to 20 keV. For each potential at each PKA energy, the statistics is based on at least 20 independent simulations (Table 1). As mentioned in the Method Section, the cluster analysis method was used to obtain the net number of defects in each defect cluster. The obtained net numbers of Frankel pairs as a function of PKA energy predicted by different modified potentials are shown in Fig. 4. It can be seen that all modified potentials predict similar numbers of Frenkel pairs as that predicted by the original CD-EAM potential when the PKA energy is equal to or lower than 10 keV, regardless of the potentials used. When the PKA energy is 20 keV, the data are a little scattered. Although the trend is not very clear, it seems that the deviation of the results from the original CD-EAM potential increases as the scaling factor deviates away from 1.0. The lowest number of Frenkel pairs is about 55 predicted by the original CD-EAM potential, and the highest number is about 75 predicted by the potential with  $SF = 0.7$ . Overall, the effect of the scaling factor on the total number of Frenkel pairs is not significant. Previously, we have shown [24] that the number of total Frenkel pairs is insensitive to the

concentration and type of solute atoms in Fe-Cr and Fe-Cu alloys. The present results are consistent with this trend, although the discrepancies increase slightly at high PKA energies. Therefore, the Fe matrix properties dominate the production of the total Frenkel pairs when the solute concentration is not very high (e.g., <15%), even if the interactions between Cr and Fe atoms are very different in these modified potentials. In addition, the results indicate that the number of total Frenkel pairs does not have a strong correlation with the heat of mixing.

#### 3.4. Production behaviors of Cr interstitials in a Fe-10%Cr alloy

Although Fig. 4 shows that the number of total surviving Frenkel pairs is insensitive to the scaling factor in the tunable potential, it is found that the production behaviors of Cr interstitials are very sensitive to the scaling factor. Fig. 5 shows three representative final defect structures of a Fe-10%Cr alloy by using three different modified potentials ( $SF = 0.9, 1.1, 1.3$ ). The PKA energy is 5 keV in each simulation. The Cr-SIA binding energies ( $E_b^{Cr-SIA}$ ) predicted by the three potentials are 0.42 eV, 0.04 eV,  $-0.32$  eV, respectively. For  $SF = 0.9$  in which  $E_b^{Cr-SIA} > 0$  (Fig. 5(a)), many Fe-Cr mixed dumbbells together with Fe SIA dumbbells survive at the end of cascade recovery stage. There are two types of mixed dumbbells [24]: Cr-interstitial-initiated and Fe-interstitial-initiated ones. In the former case, a Cr interstitial (purple) forms first then displaces a nearby Fe lattice atom to form a mixed dumbbell. As a result, a Fe vacancy (yellow) forms at the center of the mixed dumbbell. In our cluster analysis algorithm, such a Cr-interstitial-initiated mixed dumbbell is treated as a Cr interstitial. Similarly, in the latter case, a Fe interstitial (red) forms first then displaces a nearby Cr lattice atom to form a mixed dumbbell. Therefore, a Cr vacancy (green) forms at the center of the mixed dumbbell. Such a Fe-interstitial-initiated mixed dumbbell is still treated as a Fe interstitial. It can be seen that most of the mixed dumbbells are Cr-interstitial initiated ones in Fig. 5(a). For  $SF = 1.1$  in which  $E_b^{Cr-SIA} \approx 0$  (Fig. 5(b)), much fewer mixed dumbbells are produced than those with  $SF = 0.9$ . Both types of mixed dumbbells can be found in the final defect structure. For  $SF = 1.3$  in which  $E_b^{Cr-SIA} < 0$ , mixed dumbbells are barely found in the damaged structures and almost all interstitials are SIA dumbbells. A representative snapshot of the final defect structure is shown in Fig. 5(c).

Fig. 5 indicates that the fraction of Cr interstitials ( $C_{Cr}^{int}$ ) in the total interstitials may correlate with the scaling factor of the

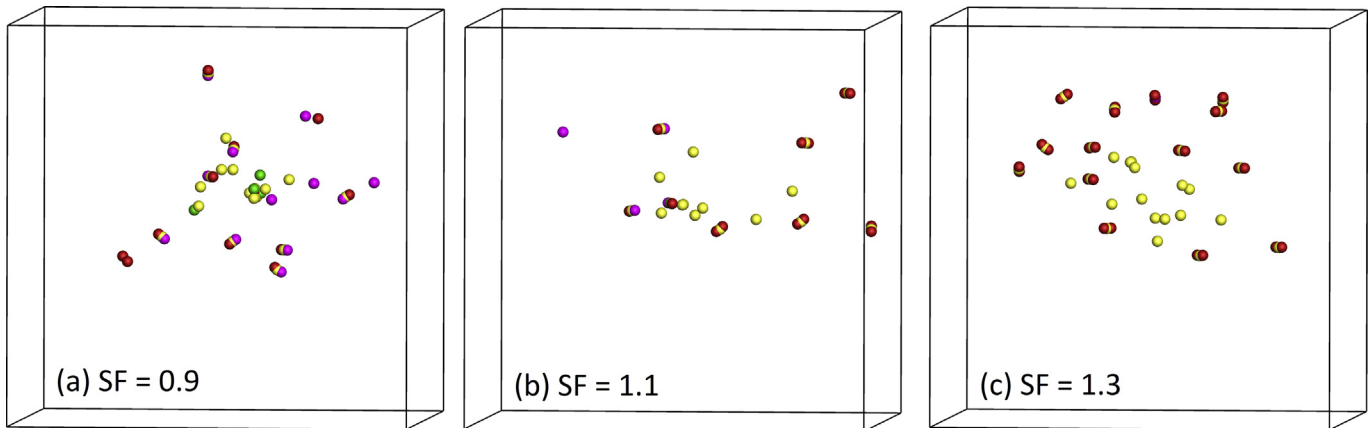


**Fig. 5.** Representative snapshots of final damage structures in a Fe-10%Cr alloy after 5 keV cascade damage. Only the defect-containing region is shown in each snapshot for clear visualization purpose. Red and purple spheres represent Fe and Cr interstitials, respectively. Yellow and green spheres represent Fe and Cr vacancies, respectively. (a)  $SF = 0.9$ ,  $E_b^{Cr-SIA} = 0.42$  eV. (b)  $SF = 1.1$ ,  $E_b^{Cr-SIA} = 0.04$  eV. (c)  $SF = 1.3$ ,  $E_b^{Cr-SIA} = -0.32$  eV. (For interpretation of the references to colour in this figure legend, the reader is referred to the Web version of this article.)

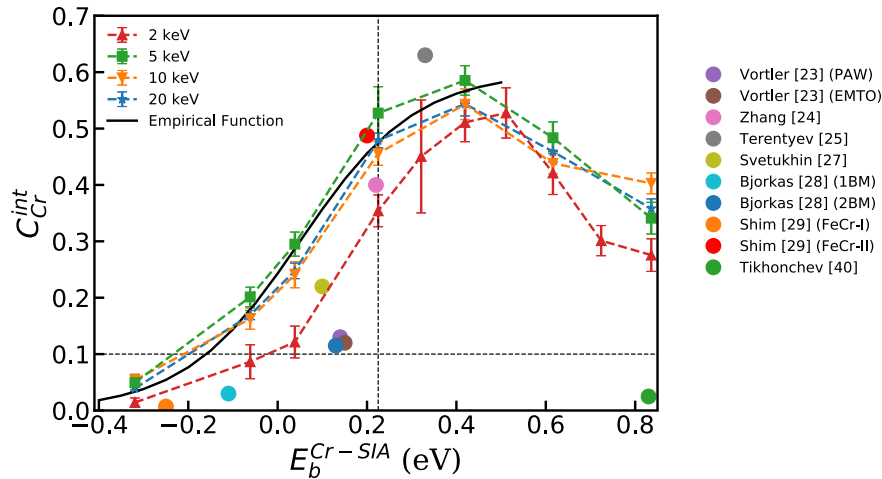


**Fig. 6.** The fractions of solute (Cr) interstitials as a function of Cr-SIA binding energy for different PKA energies predicted by the modified potentials in a Fe-10%Cr alloy. For each data point, the statistics is based on at least 20 independent simulations and the error bars represent standard errors. The filled circles represent independent cascade simulation results reported in literature. The vertical dash line indicates the results predicted by the original CD-EAM potential. The horizontal dash line indicates the Cr nominal composition (10%) in the alloy.

tunable potential, and therefore with the Cr-SIA binding energy ( $E_b^{Cr-SIA}$ ) according to Fig. 2. Here the fractions of Cr interstitials produced in the Fe-10%Cr alloy as a function of binding energy are shown in Fig. 6 for PKA energies ranging from 2 to 20 keV. Except for the 2 keV PKA energy, the results are similar for 5, 10, 20 keV PKA energies. Clearly,  $C_{Cr}^{int}$  increases with the increasing  $E_b^{Cr-SIA}$  until  $E_b^{Cr-SIA}$  reaches about 0.45 eV. Above that,  $C_{Cr}^{int}$  decreases with the increasing  $E_b^{Cr-SIA}$ . When  $E_b^{Cr-SIA} < 0$  such as -0.32 eV,  $C_{Cr}^{int}$  is very small and thus Cr interstitials are under-produced (lower than the nominal Cr concentration of 10%). This is because the formation energy of a Cr interstitial in the Fe matrix is higher (i.e., less favorable) than that of a Fe interstitial at this binding energy according to Eq. (4). When  $E_b^{Cr-SIA} \approx 0$ ,  $C_{Cr}^{int}$  is in the range between 0.1 and 0.2, depending on the PKA energies. This result indicates that when there is no binding energy between a Cr atom and a Fe SIA, or the formation energies of a Cr interstitial and a Fe SIA are the same, the Cr interstitial fraction is close to or slightly higher than the nominal Cr concentration in the alloy. In this case, the production of Cr interstitials is not biased. When  $E_b^{Cr-SIA} = 0.22$  eV, which is predicted by the original CD-EAM potential, Cr interstitial fraction is about 3.5–5.5 times of the Cr concentration in the alloy, consistent with our previous results using the same potential [24]. When  $E_b^{Cr-SIA}$  is around 0.45 eV, the Cr interstitial fraction reaches a maximum, about 5–6 times of the Cr concentration in the alloy.

When  $E_b^{Cr-SIA} > 0.45$  eV, the Cr interstitial fraction decreases with the increasing  $E_b^{Cr-SIA}$ . We find that this is due to the choice of cut-off distance for the defect characterization in the reference lattice method. Here for consistency, we use 0.9 Å for all defect analysis studies. However, as the binding energy between a Cr atom and a SIA increases, the SIA and Cr in a mixed dumbbell get closer and the defect structure is similar to a crowdion. As a result, some Cr interstitials are treated as lattice atoms because their displacements from a lattice site are less than 0.9 Å. However, if the cut-off distance is changed to 0.7 Å, the  $C_{Cr}^{int}$  calculated by the defect characterization algorithm is about 60% for modified potentials with SF=0.8, 0.7 ( $E_b^{Cr-SIA} = 0.62, 0.83$  eV). This means that Cr interstitials eventually become saturated at high binding energies.

In this work, we only focus on the results for  $E_b^{Cr-SIA} < 0.5$  eV because this binding energy is already very high. In most Fe-based alloys, the solute atoms may not have such a high binding energy with Fe SIAs. In the range of  $-0.4$  eV  $< E_b^{Cr-SIA} < 0.5$  eV, the fraction

of the Cr interstitials can be empirically fitted to a Fermi-Dirac-distribution-like equation,

$$C_{Cr}^{int} = \frac{A}{1 + \exp[-(E - E_0)/B]}, \quad (6)$$

where  $A = 0.6$ ,  $B = 0.13$ ,  $E_0 = 0.05$ . Equation (6) is plotted in Fig. 6 as the black solid line. Using this analytical equation, one may estimate the solute interstitial fraction in Fe-based alloys simply based on the solute-SIA binding energy without doing any cascade simulations. Note that the solute-SIA binding energy can be conveniently calculated with DFT calculations. For example, according to the DFT calculation [35],  $E_b^{Cr-SIA}$  is about 0.08 eV. Based on Eq. (6), we can estimate that the Cr interstitial fraction is around 30% in a Fe-10%Cr alloy for PKA energies above 5 keV.

As mentioned in the Introduction Section, previously many researchers have studied cascade-induced defect production in Fe-Cr alloys. Table 2 summarizes the simulation conditions and results in these independent studies. Here only the results at 5 keV PKA energy are shown. It is worth noting that researchers conducted these simulations using different interatomic potentials, PKA directions, simulation temperatures, defect characterization algorithms, etc. Therefore, the results are very scattered. Both over- and under-production of Cr interstitials have been reported. However, we found that most of these literature results align well with the correlation between  $C_{Cr}^{int}$  and  $E_b^{Cr-SIA}$  obtained from this work. These literature results are shown as filled circles in Fig. 6. The only exception is the work by Tikhonchev et al. [40]. In this work, the authors used a Finnis-Sinclair type potential. They reported that the formation energy of a  $\langle 110 \rangle$  Fe-Cr mixed dumbbell is 2.76 eV. The formation energy of a Fe SIA is 3.59 eV based on the potential developed by Ackland et al. [41]. Therefore, the  $E_b^{Cr-SIA}$  is about 0.83 eV. According to our correlation, the Cr interstitials should be over-produced. However, the  $C_{Cr}^{int}$  is only about 2.5% as reported in their work. It is possible that the authors did not calculate the formation energy of the  $\langle 110 \rangle$  mixed dumbbell correctly, or we misinterpreted their results. The good agreement between most of the literature results and this work demonstrates that the correlation between  $C_{Cr}^{int}$  and  $E_b^{Cr-SIA}$  indeed governs the solute interstitial production behaviors. It also demonstrates that the correlation is not specific to the modified potentials used in this work.

**Table 2**

Summary of the production behaviors of solute (Cr) interstitials in Fe–Cr alloys reported in literature. Unless those specified differently in the table, the Cr–SIA binding energy is for a <110> mixed dumbbell. CD – concentration dependent; EAM – embedded atom method; F–S – Finnis–Sinclair; 2 B M (1 B M) – two (one) band model; EMT0 – exact muffin–tin orbital; PAW – projector augmented wave.

	Potential		T (K)	$E_{PKA}$ (keV)	%Cr	$E_b^{Cr-SIA}$ (eV) (Most stable)	$C_{Cr}^{int}$
Vortler [23]	2 B M EAM [42]	PAW	300	5	10%	0.14	13%
		EMT0	300	5	10%	0.15	12%
Zhang [24]	CD-EAM [33]		300	5	10%	0.22	40%
Terentyev [25]	EAM [31]		300	5	10%	0.33 (<111>)	63%
Svetukhin [27]	CD-EAM [32]		300	5	9%	0.1	22%
Bjorkas [28]	EAM by EMT0	2 B M [42]	300	5	10%	0.13	11.5%
		1 B M	300	5	10%	–0.11	3%
Shim [29]	F–S I		673	5	10%	–0.25 (<111>)	5%
	F–S II		673	5	10%	0.2 (<111>)	50%
Tikhonchev [40]	F–S		600	5	10%	0.83	2.5%

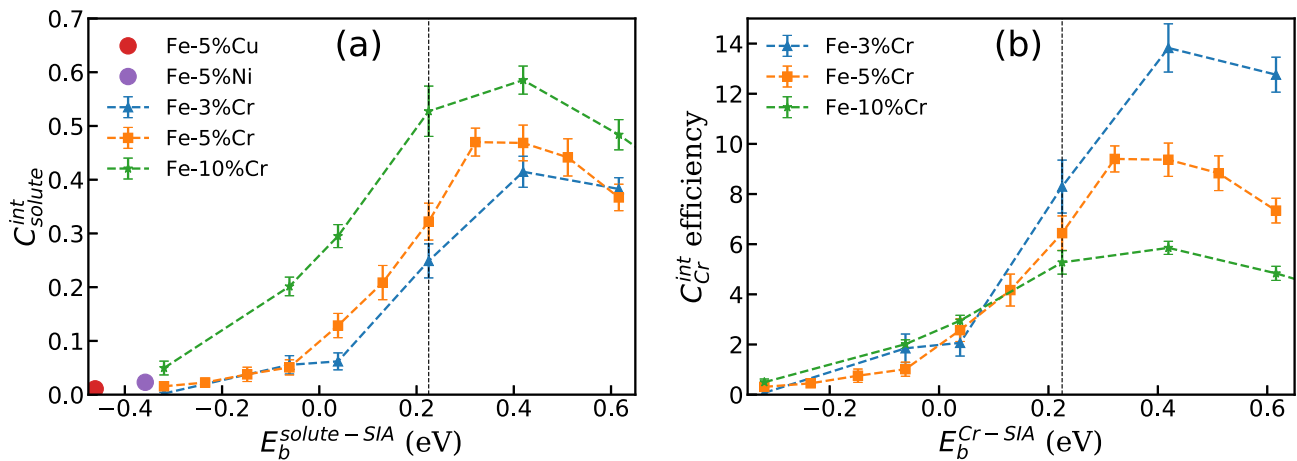


**Fig. 7.** Statistics of the solute interstitial production behaviors in Fe-based alloys of different alloy concentrations as a function of solute–SIA binding energy ( $E_b^{solute-SIA}$ ). The PKA energy is 5 keV in all simulations. The alloys are Fe–3%Cr, Fe–5%Cr, Fe–10%Cr alloys described by a series of modified potentials, and a Fe–5%Cu alloy and a Fe–5%Ni alloy. (a) Fraction of solute interstitials ( $C_{solute}^{int}$ ) in the total interstitials. (b) Solute interstitials production efficiency, which is the fraction of solute interstitials normalized by the solute nominal concentration in each alloy.

### 3.5. Production behaviors of Cr interstitials at different Cr concentrations

The production behaviors of Cr interstitials are also analyzed for Fe–Cr alloys of different Cr concentrations, including Fe–3%Cr, Fe–5%Cr, and Fe–10%Cr, with 5 keV cascade damage. The results are shown in Fig. 7. At all three Cr concentrations, the correlations between the Cr interstitial fraction and the Cr–SIA binding energy are similar: Cr interstitial fraction increases with the increasing binding energy when  $E_b^{Cr-SIA} < 0.45$  eV, as shown in Fig. 7(a). At a given binding energy, the absolute Cr interstitial fraction typically increases with the increasing Cr concentration. In order to determine whether Cr interstitials are over- or under-produced, the fraction of Cr interstitials is normalized by the Cr nominal concentration in each alloy system to get the production efficiency of Cr interstitials, as shown in Fig. 7(b). If the production efficiency is 1, the fraction of Cr interstitials is the same as the Cr nominal concentration. When  $E_b^{Cr-SIA} < 0.05$  eV, the Cr interstitial production efficiencies in the three alloys are almost the same. In this regime, Cr interstitials are under-produced or slightly over-produced because the Cr–SIA binding is weak. When  $E_b^{Cr-SIA} > 0.05$  eV, the Cr interstitial production efficiency increases sharply with the increasing Cr–SIA binding energy. Therefore, the Cr interstitials are significantly over-produced. Although the absolute Cr interstitial fraction increases with the increasing Cr nominal concentration at a given binding energy (Fig. 7(a)), the production efficiency decreases with

the increasing Cr concentration (Fig. 7(b)). This is because in concentrated alloys, the probability distribution function of Cr interstitial formation energy shifts to the higher energy side as the Cr concentration increases, as shown in our previous work [24]. As a result, the production efficiency of Cr interstitials decreases with the increasing Cr concentration.

### 3.6. Solute interstitial production behaviors in other Fe-based alloys

To verify whether the correlation between  $C_{solute}^{int}$  and  $E_b^{solute-SIA}$  shown in Fig. 7 (or Fig. 6) can be extended to other alloy systems, displacement cascade simulations were also conducted in a Fe–5% Cu alloy and a Fe–5%Ni alloy using the EAM potential that was developed for the Fe–Ni–Cu system [36]. Based on this potential, the binding energy between a Cu solute atom and a Fe SIA ( $E_b^{Cu-SIA}$ ) is  $-0.461$  eV and that between a Ni solute atom and a Fe SIA ( $E_b^{Ni-SIA}$ ) is  $-0.358$  eV. Therefore, the formation energies of both a Cu interstitial and a Ni interstitial in a Fe matrix are higher than that of a Fe SIA. According to Fig. 7 (or Fig. 6), the solute (Cu or Ni) interstitials are expected to be under-produced. Fig. 8 shows representative final defect structures in the Fe–5%Cu and Fe–5%Ni alloys damaged by a 5 keV cascade, respectively. In both snapshots, no solute interstitials are found, i.e., all produced interstitials are Fe SIAs, like in a pure Fe. Based on the statistics of 20 independent simulations in each alloy system, the resulted  $C_{solute}^{int}$  in the two alloys are shown as filled circles in Fig. 7 (a). Clearly, the fractions of

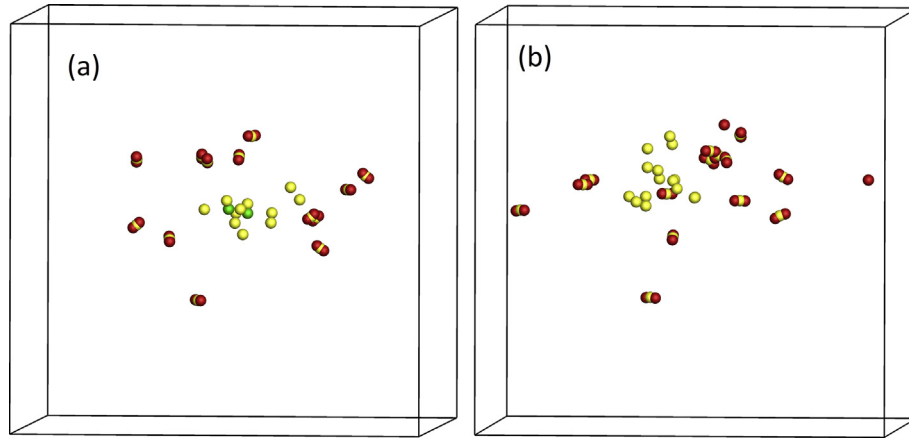


**Fig. 8.** Representative snapshots of the final damage structures in a Fe-5%Cu alloy and a Fe-5%Ni alloy upon 5 keV cascade damage. (a) Fe-5%Cu. (b) Fe-5%Ni. Red spheres represent Fe interstitials, Yellow spheres and green spheres represent Fe vacancies and solute (Cu or Ni) vacancies, respectively. Purple spheres represent solute (Cu or Ni) interstitials, although they do not appear in the two figures (because they are not produced). (For interpretation of the references to colour in this figure legend, the reader is referred to the Web version of this article.)

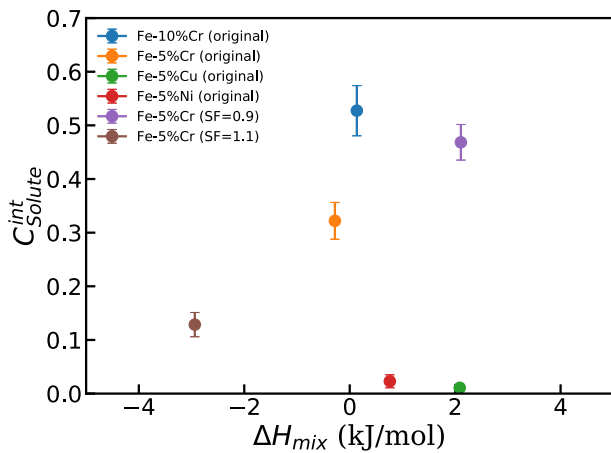


**Fig. 9.** Correlation between the solute interstitial ratio and heat of mixing for different alloys. The PKA energy is 5 keV and the statistics is based on 20 simulations for each alloy.

solute interstitials are very low in both alloys, consistent with the correlation between  $C_{solute}^{int}$  and  $E_b^{solute-SIA}$  shown in Fig. 7. Therefore, it can be reasonably speculated that the correlation between the solute interstitial fraction and the solute-SIA binding energy can be extended to a wide range of Fe-based alloys, at least semi-quantitatively.

It is worth noting that the heat of mixing does not have a clear correlation with the production behaviors of solute interstitials. To prove this, the correlation between the fraction of solute interstitials ( $C_{solute}^{int}$ ) and heat of mixing ( $\Delta H_{mix}$ ) for some alloy systems is shown in Fig. 9. The alloys are two artificial Fe-5%Cr alloys described by the modified potentials (with SF = 0.9 and SF = 1.1), and four realistic alloys described by their original potentials: Fe-5%Cr, Fe-5%Cu, Fe-5%Ni and Fe-10%Cr. The PKA energy is 5 keV in all simulations and the statistics are based on 20 independent runs in each alloy system. Clearly, no simple correlation can be established in Fig. 9. For example, the heat of mixing of the Fe-5%Cu is positive [24], which is very similar to that predicted by the modified potential with SF = 0.9. However, the solute interstitials are significantly under-produced for the Fe-5%Cu ( $E_b^{Cu-SIA} = -0.46$  eV) but over-produced for the Fe-5%Cr with SF = 0.9 ( $E_b^{Cr-SIA} = 0.42$  eV). Similarly, the solute interstitials are under-produced in the Fe-5%Ni

while its heat of mixing is positive. For the Fe-5%Cr and Fe-10%Cr alloys with the original potential, they have negative and nearly zero heat of mixing, respectively. However, the solute interstitials are over-produced in both cases. Note that for the three Fe-5%Cr alloys predicted by the modified potentials (SF = 0.9, SF = 1.1) and the original potential (SF = 1.0), the correlation with the heat of mixing seems to follow a linear trend in Fig. 9. This is likely a coincidence because the binding energies ( $E_b^{Cr-SIA}$ ) predicted by these potentials have a linear dependence with the scaling factor (Fig. 2). The dominant factor for controlling the solute interstitial production behaviors should be the solute-SIA binding energy, because a strong correlation with the binding energy can be established for different interatomic potentials and alloys, as shown in Figs. 6 and 7. In contrast, such a strong correlation cannot be established with the heat of mixing, as shown in Fig. 9.

#### 4. Conclusions and discussion

In this work, molecular dynamics simulations are conducted to study how the solute-SIA binding energy affects the production behaviors of solute interstitials during primary damage in both “real” and “artificial” Fe-Cr alloys. The concentration-dependent EAM (CD-EAM) potential [33] is used to model the “real” Fe-Cr alloys. The “artificial” Fe-Cr alloys are modeled by a series of modified potentials derived from a tunable potential, in which the Fe-Cr cross pair interaction in the original CD-EAM potential is modified by multiplying a scaling factor. The other terms in the modified potentials stay the same as the original potential, which allows us to minimize the factors that may affect the defect production behaviors. The modified potentials predict a nearly linear dependence of the Cr-SIA binding energies  $E_b^{Cr-SIA}$  (and therefore the Cr interstitial formation energy in the Fe matrix) with the scaling factor. Cascade simulations are conducted at 300 K with PKA energy ranging from 2 keV to 20 keV along the [135] direction. The alloy concentration ranges from 3% to 10%. It is found that the number of total Frenkel pairs is insensitive to the interatomic potentials, indicating that the Fe matrix dominates the production of total Frenkel pairs, at least for the alloy concentrations studied in this work. However, the fraction of solute (i.e., Cr) interstitials is very sensitive to the potentials. When the Cr-SIA binding energy is negative, the ratio of Cr interstitials to the total interstitials is lower or close to the Cr nominal concentration in the alloy; On the other hand, when the binding energy is positive, Cr interstitials are



significantly over-produced. Using the modified potentials that predict a wide range of Cr-SIA binding energies, we find that the correlation between Cr interstitial fraction and Cr-SIA binding energy ( $E_b^{Cr-SIA}$ ) follows a Fermi-Dirac-distribution-like behavior. We also summarize the Cr interstitial fractions in Fe-Cr alloys reported in literature and find that these independent results align well with the correlation obtained in this work. In addition, defect production in Fe-5%Cu and Fe-5%Ni alloys are studied and the fractions of solute interstitials in these alloys also follow this correlation, suggesting that the correlation obtained from this work may be applied to other Fe-based binary alloy systems.

This work demonstrates that the binding energy between a solute atom and a matrix SIA is a very important factor for determining the production behaviors of solute interstitials in metallic alloys. Although further studies are needed, we expect that in other binary alloys such as Ni-based alloys, a similar correlation between the solute interstitial fraction and solute-SIA binding energy also exists, as long as the solute concentration is not very high (e.g., <15%). For Fe-based alloys studied in this work, the modified potentials cover a wide range of binding energies ranging from −0.4 eV and 0.5 eV. This binding energy range covers many different Fe-based alloys. Therefore, based on the correlation obtained from this work, we may directly estimate the solute interstitial fractions during primary damage simply based on the solute-SIA binding energy without conducting laborious cascade simulations. In particular, the interatomic potentials for some Fe-based alloys are not available or may not be accurate. Using the correlation obtained from this work, the solute interstitial fractions may still be estimated semi-quantitatively, because the solute-SIA binding energies can be conveniently calculated by DFT calculations. Since the number of total Frenkel pairs produced in Fe-based alloys is similar to that in a pure Fe, regardless of solute type and composition [23,24,30], we may use the analytical NRT theory [22] to estimate the number of total Frenkel pairs and use the above correlation to further estimate the fraction of solute interstitials. The correlation may also be integrated into the widely used SRIM code [37] to predict more accurate displacements per atom (dpa) of individual alloy elements in Fe-based alloys. In SRIM calculations the displacement threshold energy is usually set to 40 eV [43] for all alloy constituents in Fe based alloys regardless of solute compositions and types. As a result, SRIM only differentiates alloy constituents based on their atomic masses and atomic numbers. This work indicates that the solute-SIA binding energy plays a dominant role and it should be included in the SRIM calculations for predicting more accurate dpas of solute elements. This work also demonstrates that the solute-SIA binding energy in an interatomic potential must be correctly fitted if one wants to use that potential to study the primary damage in metallic alloys.

In this work the Cr-SIA binding energy is tuned by modifying the Fe-Cr cross pair interaction with a scaling factor. We use this approach for convenience reasons. However, the modified potentials also change other alloy properties such as heat of mixing. Although the heat of mixing is proven to play a minor role on the solute interstitial production behaviors, it or other physical properties may have indirect effects on the final results. The current approach cannot separate such effects if they present. An alternative approach is to modify the short-range Fe-Cr cross pair interaction to limit the change of properties to interstitials. This will be a subject of future study.

#### Data availability statement

The raw/processed data required to reproduce these findings cannot be shared at this time due to technical or time limitations.

#### Acknowledgements

This work is supported by the Laboratory Directed Research and Development (LDRD) Program (16-010) at Idaho National Laboratory (Battelle Energy Alliance). Y.Z. and X.M.B. would like to thank the financial support from the LDRD Program at Idaho National Laboratory to Virginia Tech (VT fund # 418104). X.M.B. also thanks the financial support from the Faculty Joint Appointment Program at Idaho National Laboratory (VT fund # 418132) and acknowledges the Oak Ridge Associated Universities (ORAU) Ralph E. Powe Junior Faculty Enhancement Award. The authors acknowledge the use of the computing facilities at the Advanced Research Computing at Virginia Tech and the High Performance Computing at Idaho National Laboratory. This manuscript has been co-authored by Battelle Energy Alliance, LLC under Contract No. DE-AC07-05ID14517 with the U.S. Department of Energy. The United States Government retains and the publisher, by accepting the article for publication, acknowledges that the United States Government retains a nonexclusive, paid-up, irrevocable, world-wide license to publish or reproduce the published form of this manuscript, or allow others to do so, for United States Government purposes.

#### References

- [1] S.J. Zinkle, J.T. Busby, Structural materials for fission & fusion energy, *Mater. Today* 12 (11) (2009) 12–19.
- [2] S.J. Zinkle, G. Was, Materials challenges in nuclear energy, *Acta Mater.* 61 (3) (2013) 735–758.
- [3] T. Kenfield, W. Appleby, H. Busboom, W. Bell, Swelling of type-316 stainless steel at high fluences in EBR-II, *J. Nucl. Mater.* 75 (1) (1978) 85–97.
- [4] C. English, J. Hyde, Radiation Damage of Reactor Pressure Vessel Steels, *Comprehensive Nuclear Materials*, Vol 4: Radiation Effects in Structural and Functional Materials for Fission and Fusion Reactors, 2012, pp. 151–180.
- [5] R.L. Klueh, A.T. Nelson, Ferritic/martensitic steels for next-generation reactors, *J. Nucl. Mater.* 371 (1–3) (2007) 37–52.
- [6] E.A. Little, D.A. Stow, Void-swelling in irons and ferritic steels. 2. Experimental survey of materials irradiated in a fast-reactor, *J. Nucl. Mater.* 87 (1) (1979) 25–39.
- [7] F. Granberg, K. Nordlund, M.W. Ullah, K. Jin, C. Lu, H. Bei, L. Wang, F. Djurabekova, W. Weber, Y. Zhang, Mechanism of radiation damage reduction in equiatomic multicomponent single phase alloys, *Phys. Rev. Lett.* 116 (13) (2016) 135504.
- [8] Z. Li, K.G. Pradeep, Y. Deng, D. Raabe, C.C. Tansan, Metastable high-entropy dual-phase alloys overcome the strength–ductility trade-off, *Nature* 534 (7606) (2016) 227.
- [9] C. Lu, L. Niu, N. Chen, K. Jin, T. Yang, P. Xiu, Y. Zhang, F. Gao, H. Bei, S. Shi, Enhancing radiation tolerance by controlling defect mobility and migration pathways in multicomponent single-phase alloys, *Nat. Commun.* 7 (2016) 13564.
- [10] Y. Zhang, G.M. Stocks, K. Jin, C. Lu, H. Bei, B.C. Sales, L. Wang, L.K. Béland, R.E. Stoller, G.D. Samolyuk, Influence of chemical disorder on energy dissipation and defect evolution in concentrated solid solution alloys, *Nat. Commun.* 6 (2015) 8736.
- [11] F. Garner, M. Toloczko, B. Sencer, Comparison of swelling and irradiation creep behavior of fcc-austenitic and bcc-ferritic/martensitic alloys at high neutron exposure, *J. Nucl. Mater.* 276 (1–3) (2000) 123–142.
- [12] S.I. Porollo, A.M. Dvoriashin, A.N. Vorobyev, Y.V. Konobeev, The microstructure and tensile properties of Fe–Cr alloys after neutron irradiation at 400 °C to 5.5–7.1 dpa, *J. Nucl. Mater.* 256 (1998) 247–253.
- [13] S.M. Bruemmer, E.P. Simonen, P.M. Scott, P.L. Andresen, G.S. Was, J.L. Nelson, Radiation-induced material changes and susceptibility to intergranular failure of light-water-reactor core internals, *J. Nucl. Mater.* 274 (3) (1999) 299–314.
- [14] X.M. Bai, H. Ke, Y. Zhang, B.W. Spencer, Modeling copper precipitation hardening and embrittlement in a dilute Fe-0.3 at.% Cu alloy under neutron irradiation, *J. Nucl. Mater.* 495 (2017) 442–454.
- [15] E. Meslin, M. Lambrecht, M. Hernandez-Mayoral, F. Bergner, L. Malerba, P. Pareige, B. Radigue, A. Barbu, D. Gomez-Briceno, A. Ulbricht, A. Almazouzi, Characterization of neutron-irradiated ferritic model alloys and a RPV steel from combined APT, SANS, TEM and PAS analyses, *J. Nucl. Mater.* 406 (1) (2010) 73–83.
- [16] T. Toyama, A. Kuramoto, Y. Nagai, K. Inoue, Y. Nozawa, Y. Shimizu, Y. Matsukawa, M. Hasegawa, M. Valo, Effects of post-irradiation annealing and re-irradiation on microstructure in surveillance test specimens of the Lovisa-1 reactor studied by atom probe tomography and positron annihilation, *J. Nucl. Mater.* 449 (1–3) (2014) 207–212.
- [17] P.B. Wells, T. Yamamoto, B. Miller, T. Milot, J. Cole, Y. Wu, G.R. Odette, Evolution of manganese–nickel–silicon-dominated phases in highly irradiated

- reactor pressure vessel steels, *Acta Mater.* 80 (2014) 205–219.
- [18] M. Bachhav, G.R. Odette, E.A. Marquis, Alpha ' precipitation in neutron-irradiated Fe-Cr alloys, *Scripta Mater.* 74 (2014) 48–51.
  - [19] M. Bachhav, G.R. Odette, E.A. Marquis, Microstructural changes in a neutron-irradiated Fe-15 at.%Cr alloy, *J. Nucl. Mater.* 454 (1–3) (2014) 381–386.
  - [20] G.S. Was, J.P. Wharry, B. Frisbie, B.D. Wirth, D. Morgan, J.D. Tucker, T.R. Allen, Assessment of radiation-induced segregation mechanisms in austenitic and ferritic-martensitic alloys, *J. Nucl. Mater.* 411 (1–3) (2011) 41–50.
  - [21] K. Farrell, T. Byun, N. Hashimoto, Deformation mode maps for tensile deformation of neutron-irradiated structural alloys, *J. Nucl. Mater.* 335 (3) (2004) 471–486.
  - [22] R.E. Stoller, Primary Radiation Damage Formation, *Comprehensive Nuclear Materials*, Vol 1: Basic Aspects of Radiation Effects in Solids/Basic Aspects of Multi-scale Modeling, 2012, pp. 293–332.
  - [23] K. Vortler, C. Bjorkas, D. Terentyev, L. Malerba, K. Nordlund, The effect of Cr concentration on radiation damage in Fe-Cr alloys, *J. Nucl. Mater.* 382 (1) (2008) 24–30.
  - [24] Y. Zhang, D. Schwen, X.M. Bai, Molecular dynamics simulations of concentration- dependent defect production in Fe-Cr and Fe-Cu alloys, *J. Appl. Phys.* 122 (22) (2017) 225902.
  - [25] D.A. Terentyev, L. Malerba, R. Chakarova, K. Nordlund, P. Olsson, M. Rieth, J. Wallenius, Displacement cascades in Fe-Cr: a molecular dynamics study, *J. Nucl. Mater.* 349 (1–2) (2006) 119–132.
  - [26] L. Malerba, D. Terentyev, P. Olsson, R. Chakarova, J. Wallenius, Molecular dynamics simulation of displacement cascades in Fe-Cr alloys, *J. Nucl. Mater.* 329 (2004) 1156–1160.
  - [27] V. Svetukhin, M. Tikhonchev, Effective atomic displacements in Fe-9at.% Cr alloy, *Defect Diffusion Forum* 375 (2017) 139–149.
  - [28] C. Bjorkas, K. Nordlund, L. Malerba, D. Terentyev, P. Olsson, Simulation of displacement cascades in Fe90Cr10 using a two band model potential, *J. Nucl. Mater.* 372 (2–3) (2008) 312–317.
  - [29] J.H. Shim, H.J. Lee, B.D. Wirth, Molecular dynamics simulation of primary irradiation defect formation in Fe-10%Cr alloy, *J. Nucl. Mater.* 351 (1–3) (2006) 56–64.
  - [30] D. Terentyev, A. Zinovev, G. Bonny, Displacement cascades in Fe-Ni-Mn-Cu alloys: RVP model alloys, *J. Nucl. Mater.* 475 (2016) 132–139.
  - [31] V.P.R. Chakarova, J. Wallenius, Development of Fe(bcc)-cr many Body Potential and Cohesion Model, WP6 Delivery Report Nr. 6, SPIRE Project, EC Contract No. FIKW-CT-2000–20000058, June 2002. Available from: [www.neutron.kth.se/publications/library/DR-6.pdf](http://www.neutron.kth.se/publications/library/DR-6.pdf).
  - [32] A. Caro, D.A. Crowson, M. Caro, Classical many-body potential for concentrated alloys and the inversion of order in iron-chromium alloys, *Phys. Rev. Lett.* 95 (7) (2005) 075702.
  - [33] A. Stukowski, B. Sadigh, P. Erhart, A. Caro, Efficient implementation of the concentration-dependent embedded atom method for molecular-dynamics and Monte-Carlo simulations, *Model. Simulat. Mater. Sci. Eng.* 17 (7) (2009) 075005.
  - [34] S. Plimpton, Fast parallel algorithms for short-range molecular-dynamics, *J. Comput. Phys.* 117 (1) (1995) 1–19.
  - [35] P. Olsson, C. Domain, J. Wallenius, Ab initio study of Cr interactions with point defects in bcc Fe, *Phys. Rev. B* 75 (1) (2007) 014110.
  - [36] G. Bonny, R.C. Pasianot, N. Castin, L. Malerba, Ternary Fe-Cu-Ni many-body potential to model reactor pressure vessel steels: first validation by simulated thermal annealing, *Phil. Mag.* 89 (34–36) (2009) 3531–3546.
  - [37] J.F. Ziegler, *The Stopping and Range of Ions in Solids*, Ion Implantation Science and Technology, second ed., Elsevier, 1988, pp. 3–61.
  - [38] X.M. Bai, A.F. Voter, R.G. Hoagland, M. Nastasi, B.P. Uberuaga, Efficient annealing of radiation damage near grain boundaries via interstitial emission, *Science* 327 (5973) (2010) 1631–1634.
  - [39] X.M. Bai, B.P. Uberuaga, Multi-timescale investigation of radiation damage near TiO<sub>2</sub> rutile grain boundaries, *Phil. Mag.* 92 (12) (2012) 1469–1498.
  - [40] M. Tikhonchev, V. Svetukhin, A. Kadochkin, E. Gaganidze, MD simulation of atomic displacement cascades in Fe-10 at.%Cr binary alloy, *J. Nucl. Mater.* 395 (1–3) (2009) 50–57.
  - [41] G.J. Ackland, M.I. Mendelev, D.J. Srolovitz, S. Han, A.V. Barashev, Development of an interatomic potential for phosphorus impurities in alpha-iron, *J. Phys. Condens. Matter* 16 (27) (2004) S2629–S2642.
  - [42] P. Olsson, J. Wallenius, C. Domain, K. Nordlund, L. Malerba, Two-band modeling of alpha-prime phase formation in Fe-Cr, *Phys. Rev. B* 72 (21) (2005) 214119.
  - [43] ASTM E521, Standard Practice for Neutron Radiation Damage Simulation by Charged-particle Irradiation, Annual Book of ASTM Standards, Vol. 12.02, ASTM International, West Conshohocken, PA, 2009.